Sensitivity of anomalous quartic gauge couplings via $Z\gamma\gamma$ production at future hadron-hadron colliders

A. Senol,* O. Karadeniz,† K. Y. Oyulmaz,‡ C. Helveci,§ and H. Denizli¶

Department of Physics, Bolu Abant Izzet Baysal University, 14280, Bolu, Turkey

arXiv:2109.12572v4 [hep-ph] 9 Jun 2022

Abstract

Triple gauge boson production provides a promising opportunity to probe the anomalous quartic gauge couplings in understanding the details of electroweak symmetry breaking at future hadron-hadron collider facilities with increasing center of mass energy and luminosity. In this paper, we investigate the sensitivities of dimension-8 anomalous couplings related to the $ZZ\gamma\gamma$ and $Z\gamma\gamma\gamma$ quartic vertices, defined in the effective field theory framework, via $pp \to Z\gamma\gamma$ signal process with Z-boson decaying to charged leptons at the high luminosity phase of LHC (HL-LHC) and future facilities, namely the High Energy LHC (HE-LHC) and Future Circular hadron-hadron collider (FCC-hh). We analyzed the signal and relevant backgrounds via a cut based method with Monte Carlo event sampling where the detector responses of three hadron collider facilities, the center-of-mass energies of 14, 27 and 100 TeV with an integrated luminosities of 3, 15 and 30 ab^{-1} are considered for the HL-LHC, HE-LHC and FCC-hh, respectively. The reconstructed 4-body invariant mass of $l^+l^-\gamma\gamma$ system is used to constrain the anomalous quartic gauge coupling parameters under the hypothesis of absence of anomalies in triple gauge couplings. Our results indicate that the sensitivity on anomalous quartic couplings f_{T8}/Λ^4 and f_{T9}/Λ^4 (f_{T0}/Λ^4, f_{T1}/Λ^4 and f_{T2}/Λ^4) at 95 % C.L. for FCC-hh with $L_{int} = 30$ ab^{-1} without systematic errors are two (one) order better than the current experimental limits. Considering a realistic systematic uncertainty such as 10% from possible experimental sources, the sensitivity of all anomalous quartic couplings gets worsen by about 1.2%, 1.7% and 1.5% compared to those without systematic uncertainty for HL-LHC, HE-LHC and FCC-hh, respectively.

*senol_a@ibu.edu.tr

†ozgunkdz@gmail.com

‡kaan.oyulmaz@gmail.com

§helvaciceren@gmail.com

¶denizli_h@ibu.edu.tr

I. INTRODUCTION

The Standard Model (SM) puzzle was completed with the simultaneous discovery of the scalar Higgs boson, predicted theoretically in the SM, at the CERN Large Hadron Collider (LHC) by both ATLAS and CMS collaborations [1, 2]. With the discovery of this particle, the mechanism of electroweak symmetry breaking (EWSB) has become more important and still continues to be investigated. The self-interaction of the triple and quartic vector boson couplings is defined by the non-Abelian structure of the ElectroWeak (EW) sector within the framework of the SM. Any deviation in the couplings predicted by the EW sector of the SM is not observed yet with the precision measurements. While the experimental results are consistent with the couplings of $W^{\pm}$ to Z boson, there is no experimental evidence of Z bosons coupling to photons. Therefore, studying of triple and quartic couplings can either confirm the SM and the spontaneous symmetry breaking mechanism or provide clues for the new physics Beyond Standard Model (BSM). Anomalous triple and quartic gauge boson couplings are parametrized by higher-dimensional operators in the Effective Field Theory (EFT) that can be explained in a model independent way of contribution of the new physics in the BSM. The anomalous triple gauge couplings are modified by integrating out heavy fields whereas the anomalous Quartic Gauge Couplings (aQGC) can be related to low energy limits of heavy state exchange. In this scenario, the $SU(2)_L \bigotimes U(1)_Y$ is realized linearly and the lowest order Quartic Gauge Couplings are given by the dimension-eight operators [3, 4]. These operators are so-called genuine QGC operators which generate the QGC without having TGC associated with them.

Many experimental and phenomenological studies have been carried out and revealed constraints about aQGC. Both vector-boson scattering processes (i.e. $ZZjj$ and $Z\gamma jj$ process) and triboson (i.e, $Z\gamma\gamma$ production) production are directly sensitive to to the quartic $ZZ\gamma\gamma$ and $Z\gamma\gamma\gamma$ vertices. The $ZZ\gamma\gamma$ and $Z\gamma\gamma\gamma$ quartic vertices in the framework of SM are forbidden at the tree level and can only be represented by loops in higher order diagrams. Thus, the anomalous neutral QGCs parametrizing the physics beyond the SM can improve the cross section for $Z\gamma\gamma$ production and affect the kinematic distributions of the final-state Z boson and photons. Since one can fully reconstruct lepton-photon channel of the $Z\gamma\gamma$ final state and calculate the its invariant mass which is sensitive to BSM triboson contributions, we focus on the $Z\gamma\gamma$ production channel at future hadron-hadron colliders. First experimentally obtained constraint on the aQGCs via $Z\gamma\gamma$ triboson production has been reported in e^+e^- collisions at LEP [5, 6]. During the LHC Run 1, both CMS and ATLAS Collaborations have studied the $pp \to Z\gamma\gamma \to l^+l^-\gamma\gamma$ production channel using an

8 TeV data sample with an integrated luminosity of 20.3 fb^{-1} [7, 8]. The most up-to-date result for Z boson production in association with two photons is presented at a center-of-mass energy of 13 TeV with an integrated luminosity of 137 fb^{-1} in Ref. [9] by CMS collaboration. Apart from $Z\gamma\gamma$ process, the experimental studies on aQGC via three electroweak vector boson production, vector-boson scattering production of electroweak vector boson pairs have been performed at hadron colliders by the Tevatron [10, 11], the ATLAS [12–16] and CMS collaborations [17–28]. In addition to few phenomenological studies on aQGC via $Z\gamma\gamma$ production channel in the literature [29–33], there are some phenomenological studies on aQGC through the vector-boson-scattering production of electroweak vector boson pairs [34–38], the production of three electroweak vector bosons [39–43], photon-induced processes with intact protons [44–50] at hadron colliders, as well as via different production channel at $e\gamma$, $\gamma\gamma$ [51–55] and lepton colliders [56–66].

The new era starting with the novel machine configuration of the LHC and beyond aims to decrease the statistical error by increasing center of mass energy and luminosity in the measurements of the Higgs boson properties as well as finding clues to explain the physics beyond SM. With the configurations of beam parameters and hardware, the upgrade project HL-LHC will achieve an approximately 250 fb^{-1} per year to reach a target integrated luminosity of 3000 fb^{-1} at 7.0 TeV nominal beam energy of the LHC in a total of 12 years [67]. The other considered post-LHC hadron collider which will be installed in existing LHC tunnel is HE-LHC that is designed to operate at $\sqrt{s}$= 27 TeV center-of-mass energy with an integrated luminosity of at least a factor of 5 larger than the HL-LHC [68]. As stated in the Update of the European Strategy for Particle Physics by the European Strategy Group, it is recommended to investigate the technical and financial feasibility of a future hadron collider at CERN with a centre-of-mass energy of at least 100 TeV. The future project currently under consideration by CERN which comes to fore with infrastructure and technology as well as the physics opportunities is the Future Circular Collider (FCC) Study [69].

The goal of our study is to investigate the effects of anomalous quartic gauge couplings on $ZZ\gamma\gamma$ and $Z\gamma\gamma\gamma$ vertices via $pp \to Z\gamma\gamma$ process where Z boson subsequently decays to e or μ pairs at HL-LHC, HE-LHC and FCC-hh. The rest of the paper is organized as follows. A brief review of theoretical framework that discusses the operators in EFT Lagrangian is introduced in Section II. The event generation tools as well as the detail of the analysis to find the optimum cuts for separating signal events from different source of backgrounds is discussed in Section III. In section IV, we give the detail of method to obtain sensitivity bounds on anomalous quartic gauge couplings, and then determine them with an integrated luminosity L_{int} = 3 ab^{-1}, 15 ab^{-1}, 30 ab^{-1}

for HL-LHC, HE-LHC and FCC-hh, respectively. Finally, we summarize our result and compare obtained limits to the current experimental results in Section V.

II. DIMENSION-EIGHT OPERATORS FOR ANOMALOUS QUARTIC $ZZ\gamma\gamma$ AND $Z\gamma\gamma\gamma$ COUPLINGS

Although there is no contribution of the quartic gauge-boson couplings of the $ZZ\gamma\gamma$ and $Z\gamma\gamma\gamma$ vertices to the $Z\gamma\gamma$ production in the SM, new physics effects in the cross section of $Z\gamma\gamma$ production can be searched with high-dimensional effective operators which describe the anomalous quartic-gauge boson couplings without triple gauge-boson couplings. These neutral aQGCs couplings are modeled by either linear or non-linear representations using an EFT [70–72]. In the non-linear representation, the electroweak symmetry breaking is due to no fundamental Higgs scalar whereas in the linear representation, it can be broken by the conventional SM Higgs mechanism. With the discovery of the Higgs boson at the LHC, it becomes important to study the anomalous quartic gauge couplings based on linear representation. In this representation, the parity conserved and charge-conjugated effective Lagrangian include the dimension-eight effective operators by assuming the $SU(2)\times U(1)$ symmetry of the EW gauge field, with a Higgs boson belongs to a $SU(2)_L$ doublet. In this approach, the lowest dimension of operators which leads to quartic interactions but do not include two or three weak gauge boson vertices are expected to be eight. Therefore, the three classes of dimension-eight effective operators containing; i) covariant derivatives of Higgs doublet only ($\mathcal{O}_{S,j}$), ii) two field strength tensors and two derivatives of Higgs doublet ($\mathcal{O}_{M,j}$) and iii) field strength tensors only ($\mathcal{O}_{T,j}$) are added SM Lagrangian

$$\mathcal{L}_{eff} = \mathcal{L}_{SM} + \sum_{j=0}^{1} \frac{f_{S,j}}{\Lambda^4}\mathcal{O}_{S,j} + \sum_{j=0}^{7} \frac{f_{M,j}}{\Lambda^4}\mathcal{O}_{M,j} + \sum_{\substack{j=0 \\ j\neq 3}}^{9} \frac{f_{T,j}}{\Lambda^4}\mathcal{O}_{T,j} \tag{1}$$

where Λ is the scale of new physics, and $f_{S,j}$, $f_{M,j}$ and $f_{T,j}$ represent coefficients of relevant effective operators. These coefficients are zero in the SM prediction. The expanded form of these operators and a complete list of quartic vertices modified by these operators are given in Appendix A. Among the $f_{M,x}$ and $f_{T,x}$ operators that affect the $ZZ\gamma\gamma$ and $Z\gamma\gamma\gamma$ vertices, $f_{M,x}$ operators in the production of $Z\gamma\gamma$ at future of hadron-hadron colliders with high center of mass energies and luminosities were examined and their limit values were predicted in Ref[29]. Therefore, we focus on the five coefficients f_{T0}/Λ^4, f_{T1}/Λ^4, f_{T2}/Λ^4, f_{T8}/Λ^4 and f_{T9}/Λ^4 of the operators containing four field strength tensors for this study. Especially f_{T8}/Λ^4, and f_{T9}/Λ^4 give rise to only neutral anomalous quartic gauge vertices.

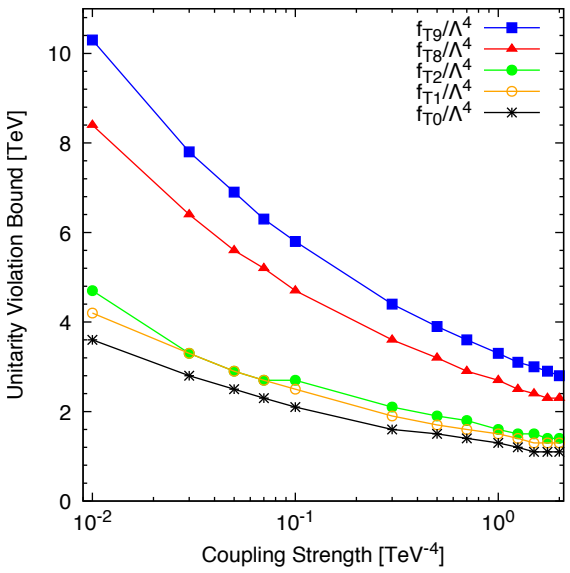


FIG. 1: The unitarity violation bound as a function of $f_{T,j}$ (where $j = 0, 1, 2, 8, 9$) aQGC via on-shell VV ($V = W/Z/\gamma$) scattering processes.

The effective field theory is only valid under the new physics scale in which unitarity violation does not occur. However, high-dimensional operators with nonzero aQGC can lead to a scattering amplitude that violates unitarity at sufficiently high energy values, called the unitarity bound. The value of the unitarity bound for the dimension-8 operators is determined by using a dipole form factor ensuring unitarity at high energies as:

$$FF = \frac{1}{(1 + \hat{s}/\Lambda_{FF}^2)^2} \tag{2}$$

where $\hat{s}$ is the maximum center-of-mass energy, Λ_{FF} is the energy scale of the form factor. The maximal form factor scale Λ_{FF} is calculated with a form factor tool VBFNLO 2.7.1 [73] for a given input of anomalous quartic gauge boson couplings parameters. The VBFNLO utility determines form factor using the amplitudes of on-shell VV scattering processes and computes the zeroth partial wave of the amplitude. The real part of the zeroth partial wave must be below 0.5 which is called the unitarity criterion. All channels the same electrical charge Q in $VV \to VV$ scattering ($V = W/Z/\gamma$) are combined in addition to individual check on each channel of the VV system. The calculated Unitarity Violation (UV) bounds using the form factor tool with VBFNLO as a function of higher-dimensional operators considered in our study are given in Fig.1. The unitarity is safe in the region that is below the line for each coefficients.

The limit values with no unitarization restriction ($\Lambda_{FF} = \infty$) on the dimension-8 aQGC (f_{T0}/Λ^4, f_{T1}/Λ^4, f_{T2}/Λ^4, f_{T8}/Λ^4 and f_{T9}/Λ^4) obtained by ATLAS and CMS collaborations by

TABLE I: The current experimental limits at 95% CL on the anomalous quartic gauge couplings f_{T0}/Λ^4, f_{T1}/Λ^4, f_{T2}/Λ^4, f_{T8}/Λ^4 and f_{T9}/Λ^4 obtained from analysis of $Z\gamma\gamma$ production as well as different production channels by ATLAS and CMS collaborations.

Collaboration	ATLAS ($\sqrt{s}$=8 TeV)	CMS ($\sqrt{s}$=13 TeV)	Current Limits by CMS ($\sqrt{s}$=13 TeV)		
Luminosity	L_{int}=20.3 fb^{-1}	L_{int}=137 fb^{-1}	L_{int}=35.9 fb^{-1}	L_{int}=137 fb^{-1}	
Channel	$Z\gamma\gamma$ [7]	$Z\gamma\gamma$ [9]	$WVjj(V = W, Z)$ [23]	$ZZjj$ [24]	$Z\gamma jj$ [28]
f_{T0}/Λ^4(TeV^{-4})	[-0.86;1.03]$\times 10^2$	[-5.70;5.46]	[-0.12;0.11]	-	-
f_{T1}/Λ^4(TeV^{-4})	-	[-5.70;5.46]	[-0.12;0.13]		-
f_{T2}/Λ^4(TeV^{-4})	-	[-11.4;10.9]	[-0.28;0.28]	-	-
f_{T8}/Λ^4(TeV^{-4})	-	[-1.06;1.10]	-	[-0.43;0.43]	-
f_{T9}/Λ^4(TeV^{-4})	[-0.74;0.74]$\times 10^4$	[-1.82;1.82]	-	-	[-0.91;0.91]

setting all other anomalous couplings to zero are summarized in Table I. The limits on f_{T0}/Λ^4, f_{T1}/Λ^4, f_{T2}/Λ^4,f_{T8}/Λ^4 and f_{T9}/Λ^4 related to the quartic $ZZ\gamma\gamma$ and $Z\gamma\gamma\gamma$ vertices have been provided by ATLAS [7](CMS [9]) collaboration at $\sqrt{s} = 8$ TeV (13 TeV) for an integrated luminosity 20.3 fb^{-1} (137 fb^{-1}) via two isolated high-energy photons and a Z boson (subsequently, decay to charged leptons) which is the signal process considered in our analysis.

The current best limits obtained by CMS collaboration for different production channels on f_{T0}/Λ^4, f_{T1}/Λ^4, f_{T2}/Λ^4, f_{T8}/Λ^4 and f_{T9}/Λ^4 couplings are also presented in last column of the Table I. The best limits obtained on f_{T0}/Λ^4, f_{T1}/Λ^4, f_{T2}/Λ^4 from WW, WZ, and ZZ boson pairs in association with two jets production [23] at a center-of-mass energy of 13 TeV with an integrated luminosity 35.9 fb^{-1}. They also reported limits on f_{T8}/Λ^4 from production of two jets in association with two Z boson [24] and f_{T9}/Λ^4 from electroweak production of a Z boson, a photon and two forward jets production [28] at a center-of-mass energy of 13 TeV with an integrated luminosity 137 fb^{-1}.

III. EVENT SELECTION AND DETAILS OF ANALYSIS

The details of the analysis are given for the effects of dimension-8 operators on anomalous quartic gauge boson couplings via $pp \to Z\gamma\gamma$ signal process for future hadron-hadron circular colliders in this section. The $pp \to Z\gamma\gamma$ process receives contributions from three Feynman Diagrams at the three-level as shown in Fig.2. The first two diagrams account for the anomalous quartic $ZZ\gamma\gamma$ and $Z\gamma\gamma\gamma$ couplings while the other represents the SM contribution. The green circles

indicate the vertices which are defined by the operators Eqs.(A3)-(A19) in the Lagrangian (Eq.1). The cross section and dynamical distributions are evaluated using a parton level Monte-Carlo (MC) simulations which are performed within the MadGraph5_aMC@NLO [74]. In addition, the effective Lagrangians of $ZZ\gamma\gamma$ and $Z\gamma\gamma\gamma$ anomalous quartic couplings are implemented into MadGraph5_aMC@NLO based on FeynRules [75] and Universal FeynRules Output (UFO) framework [76]. In our Leading-Order (LO) cross section calculations at the generator level to consider the finite acceptance of the detectors and isolation of the final state observable particles, we applied cuts on pseudo-rapidity of photons as $|\eta^{\gamma}| < 2.5$ and on separation of two photon in the pseudorapidity-azimuthal angle plane as $\Delta R(\gamma,\gamma) > 0.4$. Additionally, we introduced a generator level cut on the transverse momentum of the photons not only to guarantee that our results are free of infrared divergences but also to improve event generating efficiency. In order to determine transverse momentum cut on final state photons at generator level, the cross section of $Z\gamma\gamma$ process as a function of the lower cut on photon transverse momentum are plotted for HL-LHC ($\sqrt{s}$=14 TeV), HE-LHC($\sqrt{s}$=27 TeV) and FCC-hh ($\sqrt{s}$=100 TeV) colliders in the first row of Fig 3, respectively. The cross sections with one non-zero anomalous quartic gauge couplings at a time as well as SM are selected in these figures for the illustrative purpose. As seen from these figures, $p_T^{\gamma} > 15$ GeV for HL-LHC and HE-LHC, $p_T^{\gamma} > 25\ GeV$ for FCC-hh are chosen for further analysis. The second row of Fig.3 shows the production cross section of the $Z\gamma\gamma$ process in terms of the anomalous quartic gauge couplings for three different hadron-hadron collider options with corresponding generator level cuts. Each line in the second row of Fig. 3 corresponds to variation of cross section with respect to one of the coupling while others are kept at zero. The sensitivity of f_{T8}/Λ^4 and f_{T9}/Λ^4 anomalous quartic couplings for each collider options to cross sections is more significant than the other couplings as seen in the second row of Fig. 3. Therefore, we expect to obtain better limits on the f_{T8}/Λ^4 and f_{T9}/Λ^4 couplings with $Z\gamma\gamma$ production. The general expression for amplitude in the EFT regime for the process considered can be written as

$$|M_{SM} + M_{dim8}|^2 = \underbrace{|M_{SM}|^2}_{\mathcal{O}(\Lambda^0)} + \underbrace{2\Re\left(M_{SM}M_{dim8}^*\right)}_{\mathcal{O}(\Lambda^{-4})} + \underbrace{|M_{dim8}|^2}_{\mathcal{O}(\Lambda^{-8})} \tag{3}$$

where $|M_{SM}|^2$, $\Re\left(M_{SM}M_{dim8}^*\right)$ and $|M_{dim8}|^2$ are the SM, interference of the SM amplitude with higher dimensional operators, and the square of the new physics contributions, respectively. In order to show the effectiveness of the form factor, the cross sections at LO without and with Λ_{FF}=1.5 and 2 TeV is presented for all three collider options in Fig.4. It can be clearly seen in Fig. 4 that the square contributions of the new physics amplitudes suppress the interference contributions of the SM amplitude with high-dimensional operators in the case where the UV limit is not applied.

However, if the new physics energy scale is heavy (i.e. Λ_{FF}=1.5 and 2 TeV or higher), the largest new physics contribution to $pp \to Z\gamma\gamma$ process is expected from the interference between the SM and the dimension-eight operators as seen from Fig. 4.

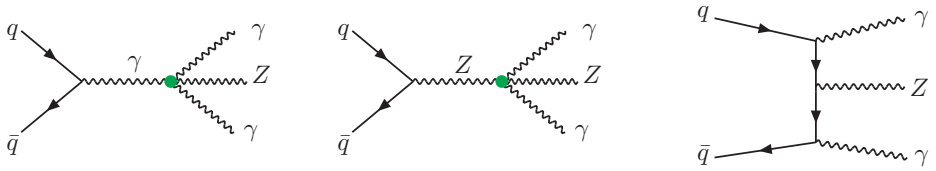


FIG. 2: Feynman diagrams for the tree-level $Z\gamma\gamma$ production of anomalous quartic gauge-boson coupling vertex (represented with green circle) and the SM contributions.

For further analysis including response of the detector effects, we generate 600k events for all backgrounds and signal processes where we scan each f_{T0}/Λ^4, f_{T1}/Λ^4, f_{T2}/Λ^4, f_{T8}/Λ^4 and f_{T9}/Λ^4 couplings with nine different values ranging from negative to positive. The generated signal and (relevant) background events with applied generator level cuts are first passed through Pythia 8.20 [77] for hadronization, parton showering and decay of unstable particles at parton level. Then hadronized events are interfaced with Delphes 3.4.2 [78] software to model response of the corresponding detector for each collider. We choose the upgraded cards namely `delphes_card_HLLHC_aqgc.tcl` and `FCC-hh.tcl` where detector response in the form of resolution functions and efficiencies are parametrised for HL-LHC, HE-LHC and FCC-hh, respectively. Jets are reconstructed by using clustered energy deposits with FastJet 3.3.2 [79] using anti-kt algorithm [80] where a cone radius is set as $\Delta R = 0.4$ (0.2) and p_T^j>15 (25) GeV for HL-LHC and HE-LHC (FCC-hh) colliders.

Our main focus is to see the effects of anomalous quartic gauge boson couplings via $pp \to Z\gamma\gamma$ signal process where Z boson subsequently decays to e or μ pairs. Therefore, events with two isolated photons and one pair of the same flavor and oppositely charged leptons (electrons or muons) are selected for further analysis (Cut-0). Electron and muon channels are combined to increase sensitivity even more. The signal includes nonzero effective couplings and SM contribution as well as its interference. "sm" stands for SM background process of the same final state with the signal process in our analysis. The main background processes to the selected $l^+l^-\gamma\gamma$ sample of events may originate from $Z\gamma j$ and Zjj production with hadronic jet misidentified as a photon. Such misidentifications generally arise from jets hadronizing with a neutral meson, which carries away most of the jet energy. The photons that carry a large fraction of the jet energy can exceed the reconstructed

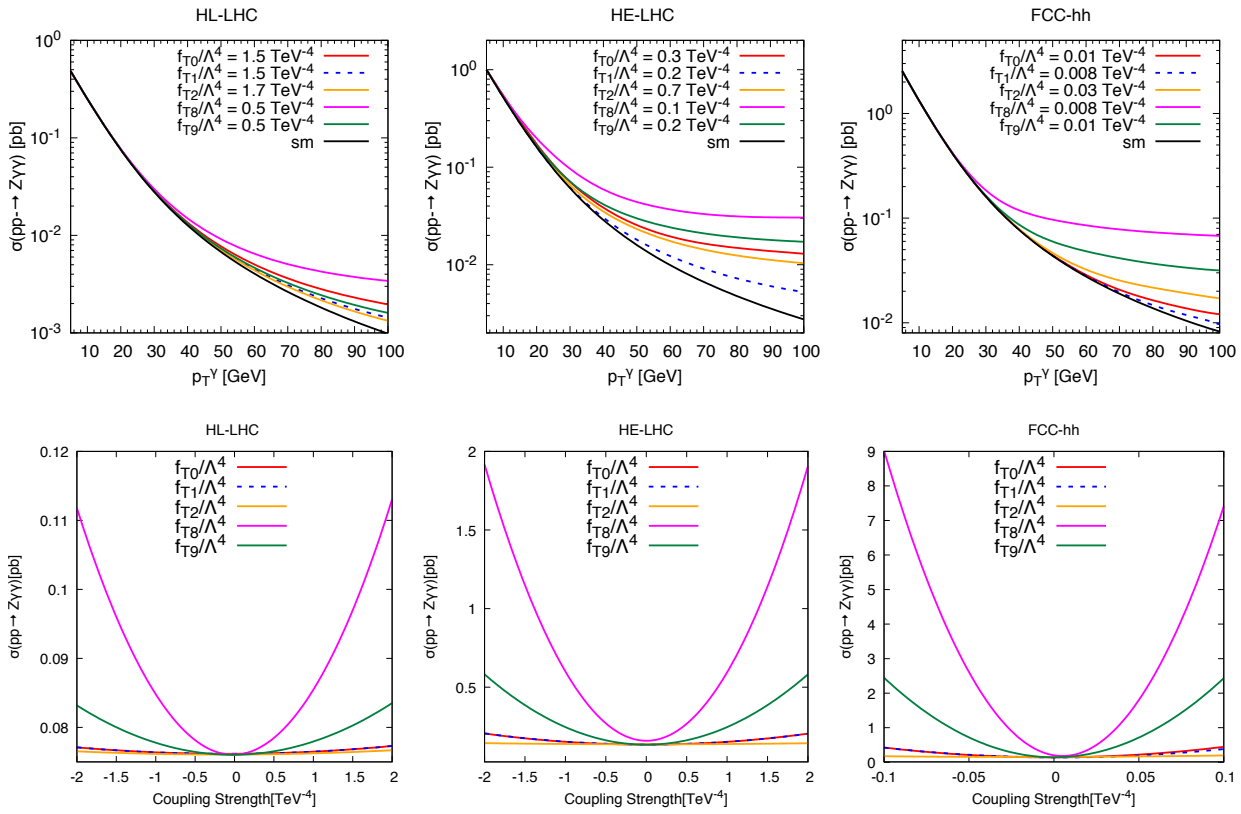


FIG. 3: In the top row the cross section of the $pp \to Z\gamma\gamma$ process as function of the lower cut on photon transverse momentum are shown while the bottom row shows production cross section of the $Z\gamma\gamma$ process in terms of the anomalous quartic gauge couplings for HL-LHC, HE-LHC and FCC-hh (left to right, respectively.)

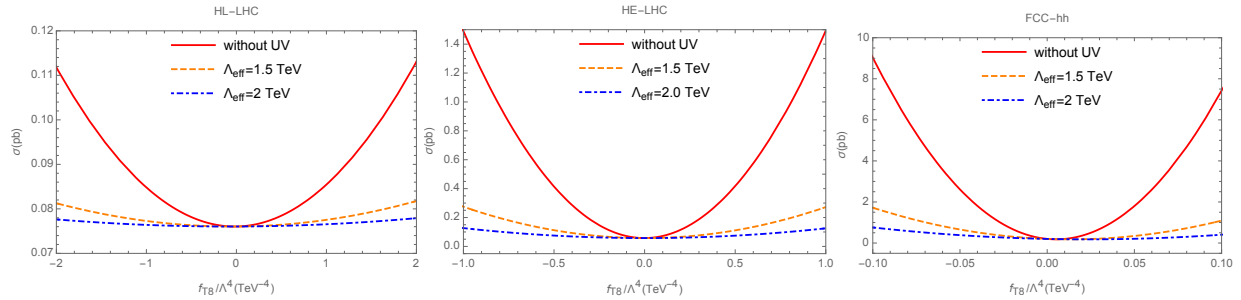


FIG. 4: The cross section of the $pp \to Z\gamma\gamma$ process as function of the anomalous quartic gauge coupling f_{T8}/Λ^4 for HL-LHC, HE-LHC and FCC-hh without UV bound applied and with form factor scale Λ_{FF}=1.5 and 2 TeV.

photon isolation requirements. The probability of misidentifying a jet as a photon depends on how the jets interact with the detector. Due to the great angular resolution of existing calorimeters in current LHC detectors, the probability of a hard scattering jet being mis-reconstructed as an

TABLE II: Event selection criteria and applied kinematic cuts for the analysis of the HL-LHC, HE-LHC and FCC-hh collider options

Cuts	HL-LHC	HE-LHC	FCC-hh
Cut-0	$N_l \geqslant 2$ and same flavour but opposite charge, $N_\gamma \geqslant 2$		
Cut-1	$p_T^{l_1,l_2} > 25$ GeV, $\lvert\eta^{l_1,l_2}\rvert \leqslant 2.5$		
Cut-2	$p_T^{\gamma_1,\gamma_2} > 15$ GeV, $\lvert\eta^{\gamma_1,\gamma_2}\rvert \leqslant 2.5$	$p_T^{\gamma_1,\gamma_2} > 20$ GeV, $\lvert\eta^{\gamma_1,\gamma_2}\rvert \leqslant 2.5$	$p_T^{\gamma_1,\gamma_2} > 20$ GeV, $\lvert\eta^{\gamma_1,\gamma_2}\rvert \leqslant 2.5$
Cut-3	$\Delta R(\gamma_1,\gamma_2) > 0.4$, $\Delta R(\gamma_1,l_1) > 0.4$, $\Delta R(l_1,l_2) < 1.4$		
Cut-4	81 GeV $< M_{l^+l^-} <$ 101 GeV		
Cut-5	$p_T^{\gamma_1} > 160$ GeV	$p_T^{\gamma_1} > 250$ GeV	$p_T^{\gamma_1} > 300$ GeV

isolated photon is low. The granularity for the detectors of future hadron-hadron colliders, for which we will use detector parameters, is expected to be 2-4 times better than current LHC detectors. Therefore, we applied the same rate as in the HL-LHC detectors for all colliders options in a fake-rate of jet-photon which can be parametrized in the form $\epsilon_{j\to\gamma} = 0.0007 \cdot e^{-p_T[GeV]/187}$ [81, 82]. The remaining minor background contributions are originated from WZ, ZZ and $\tau^+\tau^-\gamma\gamma$ processes. WZ and ZZ backgrounds are considered either the electrons from the decay of the W and Z boson are misidentified as photons or final state photons are radiated. $\tau^+\tau^-\gamma\gamma$ has also the same final state as the considered signal process. In our analysis, we will use the traditional cut-based method to obtain the best possible bounds for anomalous quartic gauge couplings. This method is based on determining the optimum kinematic cuts from the kinematic distributions of the final state particles in the selected events and then maximizing the number of signal events with a powerful single kinematic observable that can distinguish between the signal and the background using these cuts. The charged leptons (photons) in the final state are ordered with respect to their transverse momenta; the leading and sub-leading as l_1 (γ_1) and l_2 (γ_2), respectively. All kinematical distributions are normalized to the number of expected events (cross section of each process times the integrated luminosity L_{int} = 3 ab^{-1}, 15 ab^{-1}, 30 ab^{-1} for HL-LHC, HE-LHC and FCC-hh, respectively). The normalized distributions of the transverse momentum as well as pseudo-rapidity of leading and sub-leading charged leptons and photons in the selected events (Cut-0) for signal and relevant backgrounds are shown in Fig. 5 (Fig.8) and Fig.6 (Fig.9) for HL-LHC (FCC-hh) options, respectively. Similar distribution have also been obtained for HE-LHC. By considering typical requirements of the experimental detectors and normalized distributions of final state leptons and photons, we impose minimal cuts on the transverse momentum and rapidity of

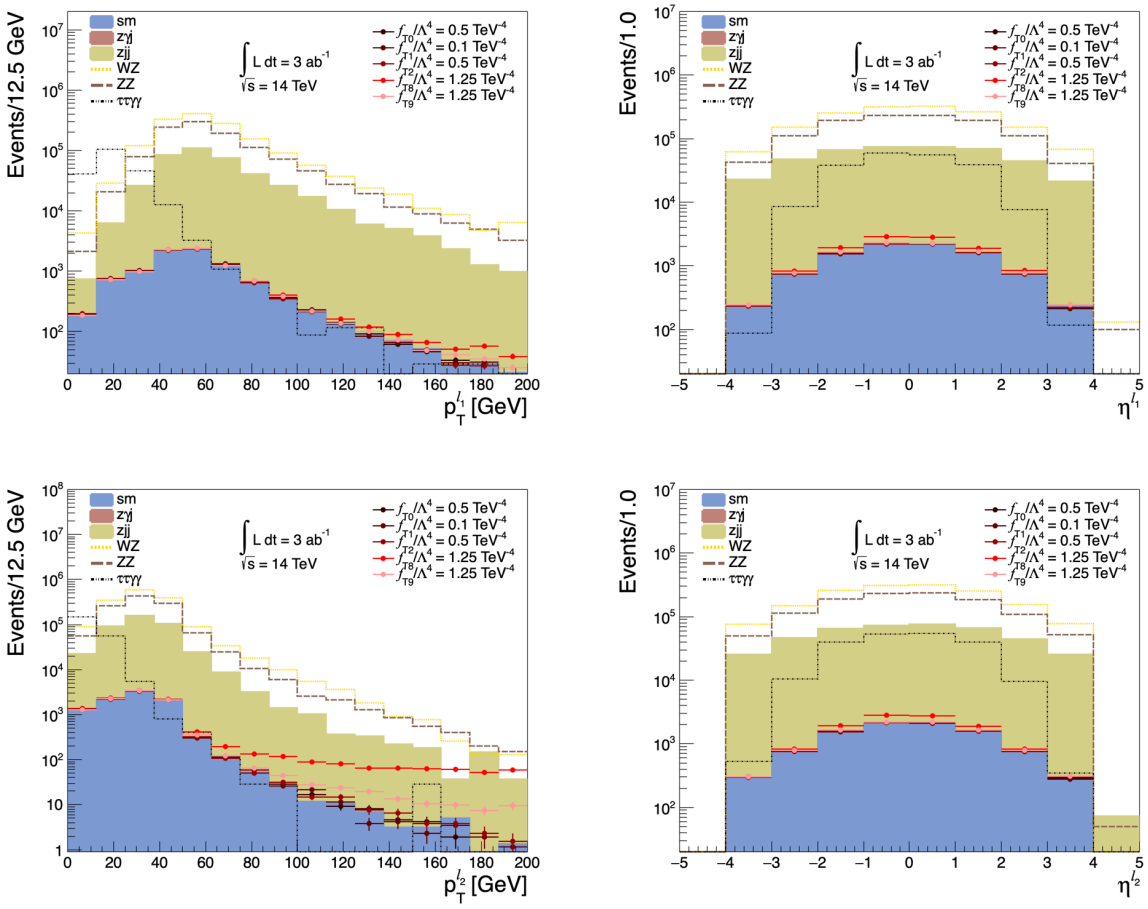


FIG. 5: Normalized distributions of transverse momentum and pseudo-rapidity of the leading (l_1) and sub-leading leptons (l_2) after the event selection (Cut-0) for the signals and all relevant backgrounds processes at HL-LHC with L_{int}=3 ab^{-1}.

the final-state charged leptons and photons as given Cut-1 and Cut-2 in Table II for each collider options. Since the signal event contains two photons, we can safely suppress the event contamination and avoid infrared divergences by using a minimum transverse momentum and pseudo-rapidity cuts of the leading and sub-leading photons for the other background processes. Furthermore, the normalized distributions of leading and sub-leading photons ($\Delta R(\gamma_1, \gamma_2)$), leading photon and leading charged lepton ($\Delta R(\gamma_1, l_1)$), leading and sub-leading charged leptons ($\Delta R(l_1, l_2)$) separation in the pseudorapidity-azimuthal angle plane as well as the invariant mass of the oppositely signed charged lepton pair are given in Fig.7 (Fig.10) for HL-LHC (FCC-hh). To have well-separated photons and charged leptons in the phase space that leads to be identified separate objects in the detector, we require separations as $\Delta R(\gamma_1, \gamma_2) > 0.4$, $\Delta R(\gamma_1, l_1) > 0.4$ and $\Delta R(l_1, l_2) < 1.4$ (Cut-3). We also impose the invariant mass window cut around the Z boson mass peak as 81 GeV

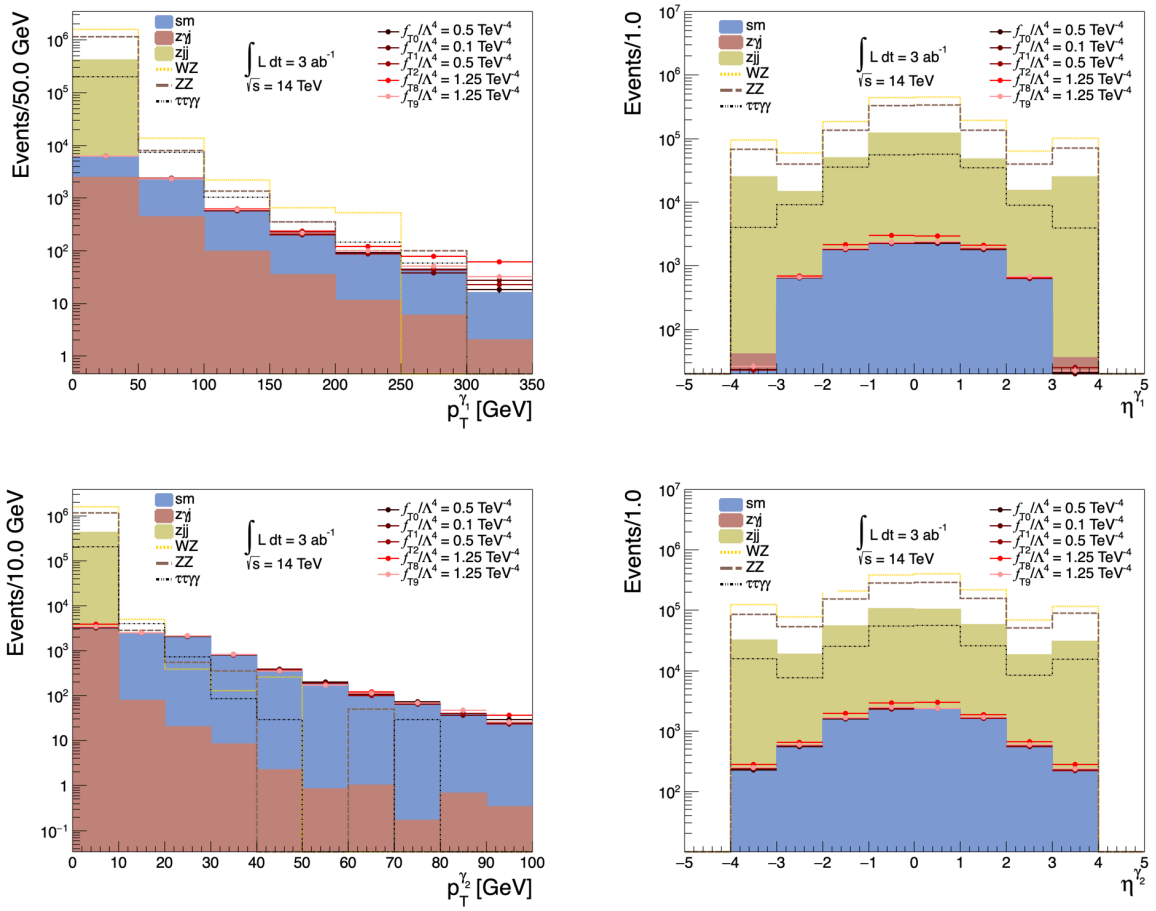


FIG. 6: Normalized distributions of transverse momentum and pseudo-rapidity of the leading (γ_1) and sub-leading leptons (γ_2) after the event selection (Cut-0) for the signals and all relevant backgrounds processes at HL-LHC with $L_{int} = 3$ ab^{-1}.

$< M_{l^+l^-} <$ 101 GeV (Cut-4) to suppresses the virtual photon contribution to the di-lepton system. Since requiring the high transverse momentum photon eliminates the fake backgrounds, we plot the transverse momentum of leading photon for HL-LHC, HE-LHC and FCC-hh in Fig.11 (left to right) to define a region which is sensitive to aQGC. From these normalized plots we apply a cut on $p_T^{\gamma_1}$ as 160 GeV, 250 GeV and 300 GeV for each collider option, respectively (Cut-5). The flow of cuts are summarized in Table II for each hadron-hadron colliders that we analyzed. The normalized number of events after applied cuts are presented in Table III to demonstrate the effect of the cuts used in the analysis for signal (f_{T8}/Λ^4=0.7, 0.07 and 0.01 TeV $^{-4}$ chosen for illustrative purpose) and relevant backgrounds. The number of events in this table are normalized to the cross section of each process times the corresponding integrated luminosity for each collider options, L_{int} = 3, 15 and 30 ab^{-1} for the HL-LHC, HE-LHC and FCC-hh, respectively. We apply a fake-rate of

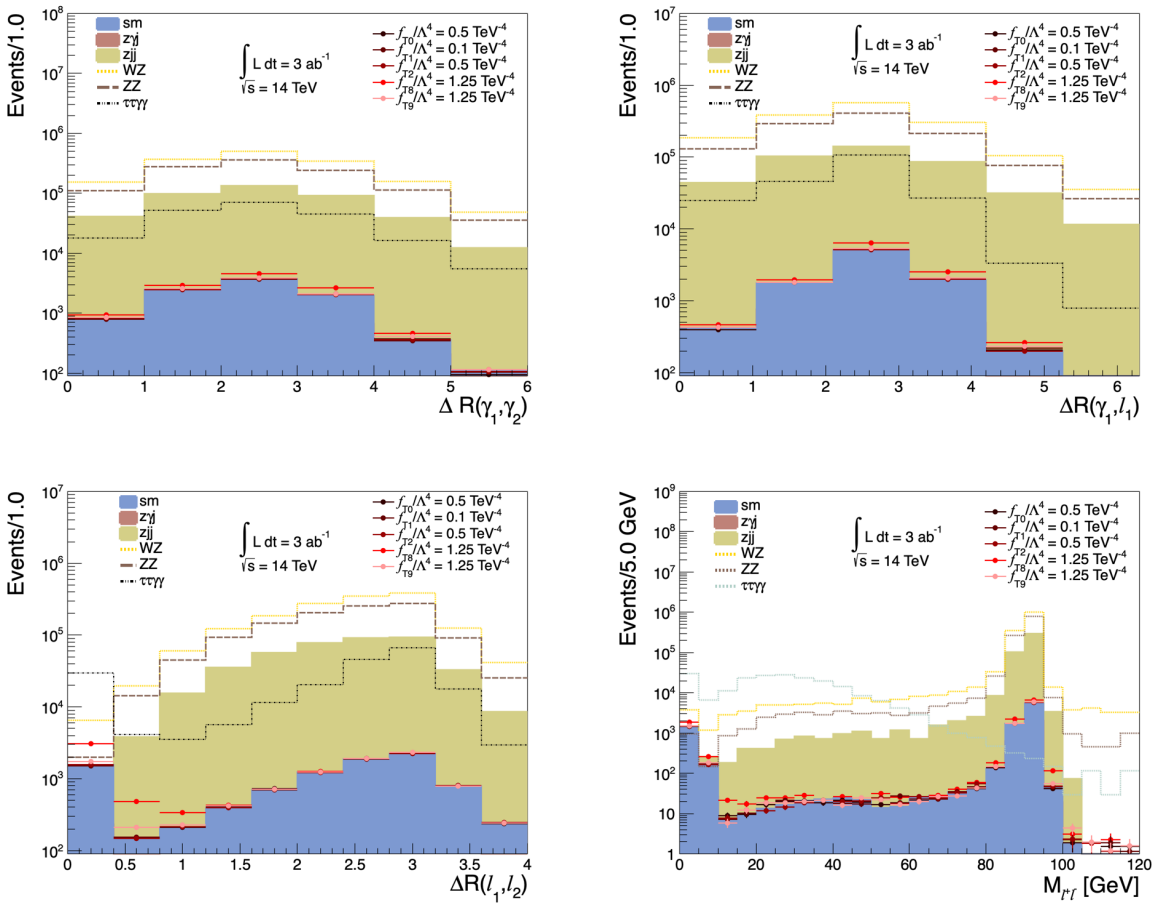


FIG. 7: Normalized $\Delta R(\gamma_1, \gamma_2)$, $\Delta R(\gamma_1, l_1)$, $\Delta R(l_1, l_2)$ and charged lepton pair invariant mass distribution for the signals and all relevant backgrounds processes at HL-LHC with $L_{int} = 3\text{ab}^{-1}$

jet-photon $\epsilon_{j\to\gamma} = 0.0007 \cdot e^{-p_T[GeV]/187}$ for $Z\gamma j$ and Zjj backgrounds as discussed previously. As it can be noticed in this table, all other relevant backgrounds are reduced more than signal and *sm* background. Overall cut efficiencies of our study are 3.6% and 1.3% for signal and *sm* background at HL-LHC option while they are 1.1% and 0.64% at HE-LHC and 1.5% and 0.63% at FCC-hh option.

IV. SENSITIVITY OF ANOMALOUS QUARTIC GAUGE COUPLINGS FOR HL-LHC, HE-LHC AND FCC-HH

In this section, we discuss the detail of the method to obtain sensitivity bounds on anomalous quartic gauge couplings, and then determine the bounds on f_{T0}/Λ^4, f_{T1}/Λ^4, f_{T2}/Λ^4, f_{T8}/Λ^4 and f_{T9}/Λ^4 with an integrated luminosity $L_{int} = 3$ ab^{-1}, 15 ab^{-1}, 30 ab^{-1} for HL-LHC, HE-LHC

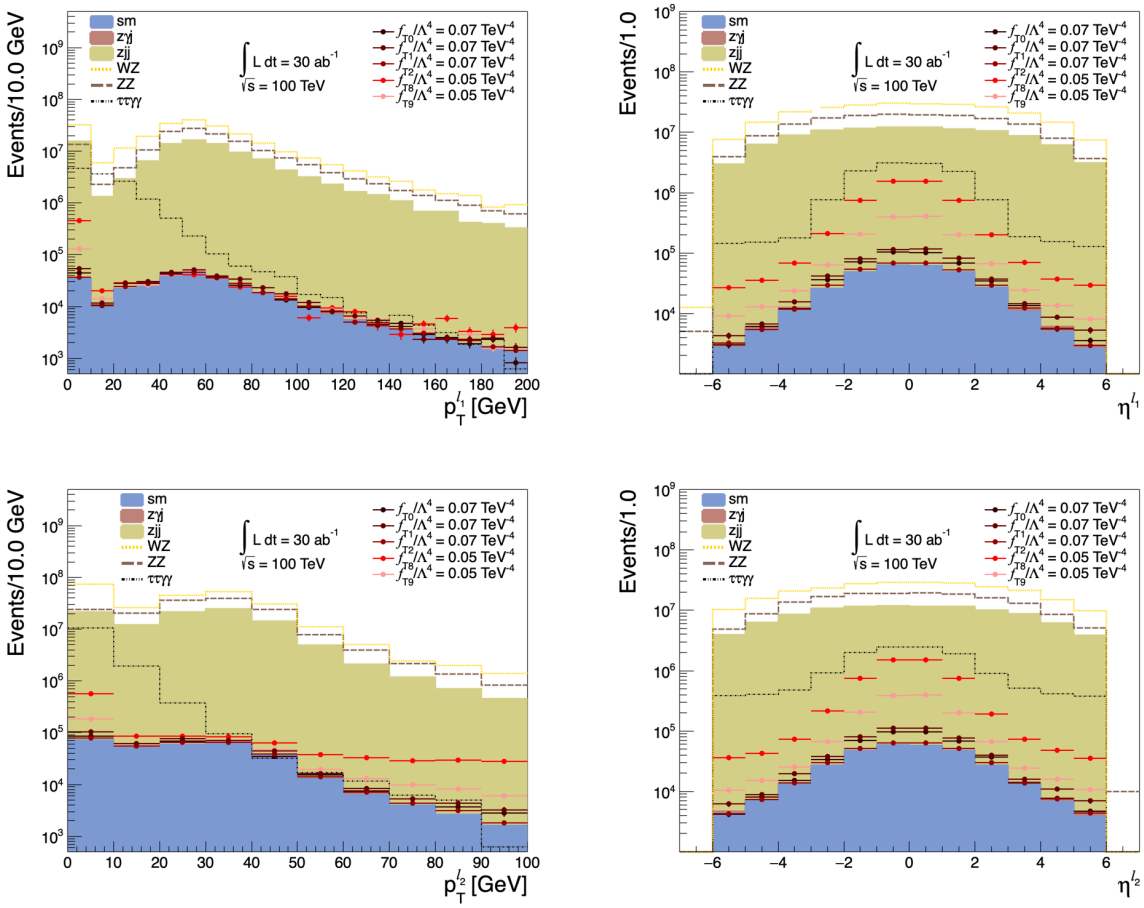


FIG. 8: Normalized distributions of transverse momentum and pseudo-rapidity of the leading (l_1) and sub-leading leptons (l_2) after the event selection (Cut-0) for the signals and all relevant backgrounds processes at FCC-hh with $L_{int} = 30$ ab^{-1}.

and FCC-hh, respectively. The distribution of the reconstructed 4-body invariant mass of $l^+l^-\gamma\gamma$ system for HL-LHC, HE-LHC and FCC-hh options given in Fig. 12 (top to bottom, respectively). is used to constrain the aQGC parameters under the hypothesis of absence of anomalous triple gauge couplings. The contribution of aQGCs is more visible at high values of the reconstructed 4-body invariant mass of $l^+l^-\gamma\gamma$ system. The effect of UV bound is also presented in this figure where the distributions with (without) UV bound is on the right (left). The UV bounds are determined by Fig.1 where it is related to the strength of the aQGCs (e.g., the UV bound values for f_{T8}/Λ^4 coupling values of 1.25 TeV^{-4}, 0.5 TeV^{-4} and 0.01 TeV^{-4} are 2.5 TeV, 3.2 TeV and 8.4 TeV). As seen from Fig.12, the applied UV bounds impose an upper-cut in the invariant mass of the $l^+l^-\gamma\gamma$ system which guarantees that the unitarity constraints are always satisfied. The number of events after applying UV bounds for signals are given in the parenthesis at Table III for comparison

TABLE III: The cumulative number of events for signal (f_{T8}/Λ^4=0.7, 0.07 and 0.01 TeV $^{-4}$) and relevant background processes after applied cuts. The numbers are normalized to the cross section of each process times the integrated luminosity, L_{int} = 3 ab^{-1}, 15 and 30 ab^{-1} for the HL-LHC, HE-LHC and FCC-hh respectively. The number of events between the parenthesis are obtained after applying UV bounds for signals. We apply a fake-rate of jet-photon $\epsilon_{j\to\gamma} = 0.0007 \cdot e^{-p_T[GeV]/187}$ for $Z\gamma j$ and Zjj backgrounds.

Cuts	signal	sm	$Z\gamma j$	Zjj	WZ	ZZ	$\tau\tau\gamma\gamma$
	f_{T8}/Λ^4=0.7 TeV $^{-4}$			HL-LHC			
Cut-0	10012 (9869)	9502	3027	420661	1599830	1161880	209514
Cut-1	5277 (5117)	4914	1610	212264	871430	640538	6860
Cut-2	3528 (3385)	3293	29	78892	392	600	87
Cut-3	420 (378)	168	2	0	0	0	0
Cut-4	381 (353)	128	1	0	0	0	0
Cut-5	366 (230)	124	1	0	0	0	0
	f_{T8}/Λ^4= 0.07 TeV $^{-4}$			HE-LHC			
Cut-0	84234 (84144)	83075	35191	5768510	17932500	13334500	1828320
Cut-1	43192 (43113)	42920	18435	2785550	90355710	6905490	65364
Cut-2	18817 (18744)	18724	162	510	0	5666	0
Cut-3	2554 (2483)	2369	36	0	0	1700	0
Cut-4	2448 (2376)	2290	28	0	0	567	0
Cut-5	682 (609)	516	4	0	0	0	0
	f_{T8}/Λ^4=0.01 TeV $^{-4}$			FCC-hh			
Cut-0	339659 (336093)	316474	277688	104987000	255968000	162914000	13170400
Cut-1	135863 (132902)	125512	108020	29593500	66414700	52153500	280985
Cut-2	84834 (82976)	79066	793	0	24973	14963	0
Cut-3	19272 (17494)	16211	198	0	12486	0	0
Cut-4	18467 (16848)	15585	149	0	12486	0	0
Cut-5	5205 (4010)	2958	20	0	0	0	0

purpose.

In order to obtain a continuous prediction for the anomalous quartic gauge couplings after Cut-5, a quadratic fit is performed to number of events for each couplings ($\sum_i^{n_{bins}} N_i^{NP}$) obtained by integrating the invariant mass distribution of $l^+l^-\gamma\gamma$ system in Fig.12. The obtaining of the 95% Confidence Level (C.L.) limit on a one-dimensional aQGC parameter is performed by χ^2 test which corresponds to 3.84

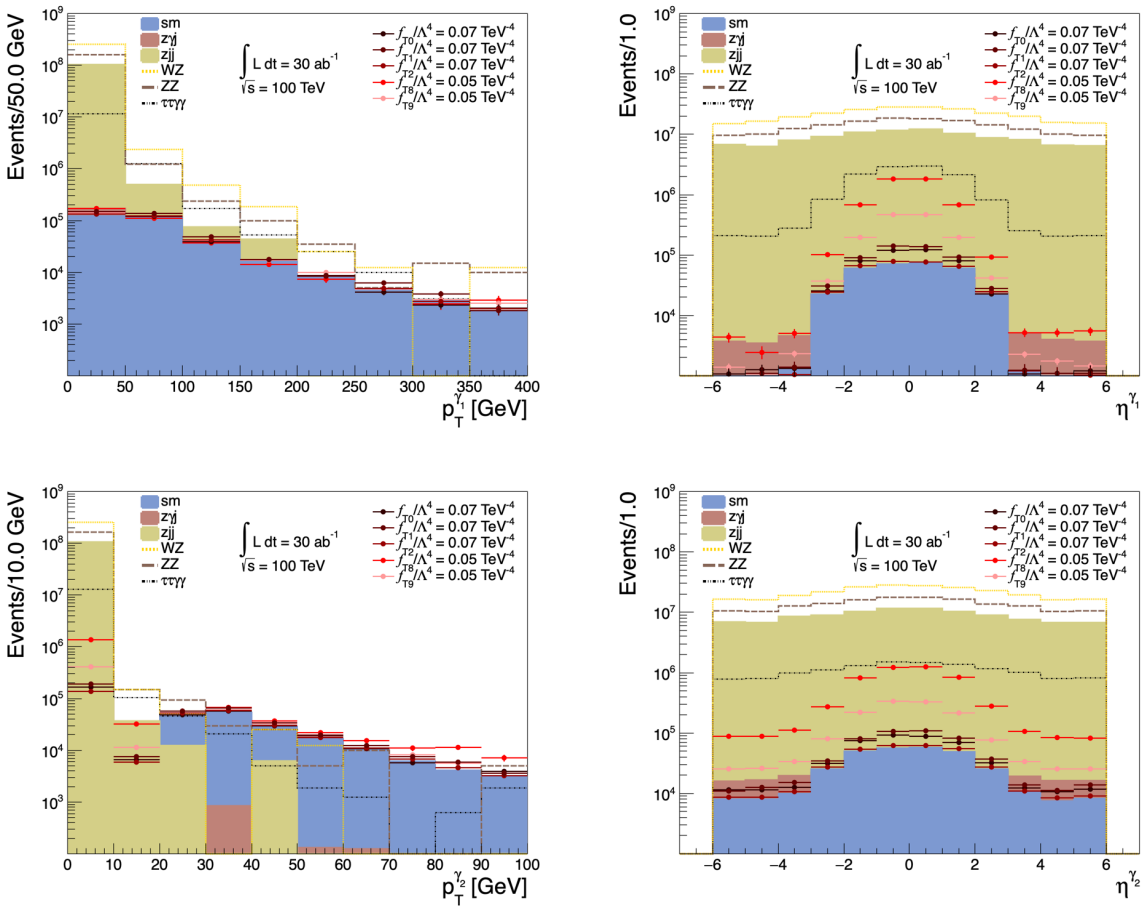


FIG. 9: Normalized distributions of transverse momentum and pseudo-rapidity of the leading (γ_1) and sub-leading leptons (γ_2) after the event selection(Cut-0) for the signals and all relevant backgrounds processes at FCC-hh with $L_{int} = 30$ ab^{-1}

$$\chi^2 = \sum_i^{n_{bins}} \left(\frac{N_i^{NP} - N_i^B}{N_i^B \Delta_i} \right)^2 \tag{4}$$

where N_i^{NP} is the total number of events in the existence of aQGC, N_i^B is total number of events of the corresponding SM backgrounds in ith bin, $\Delta_i = \sqrt{\delta_{sys}^2 + \frac{1}{N_i^B}}$ is the combined systematic (δ_{sys}) and statistical uncertainties in each bin.

The sensitivities of the aQGCs can exhibit in two ways; i) allowing the collider to probe sensitivity to new physics above the unitary bound by measuring the direct generation of new resonances and their couplings; ii) assuming that the new physics is probed "virtually" by high-dimension operators that only contain SM fields, and ensuring that the generated events remain below the unitary bounds in the di-boson mass. The 95% C.L. limits of the aQGCs obtained by varying

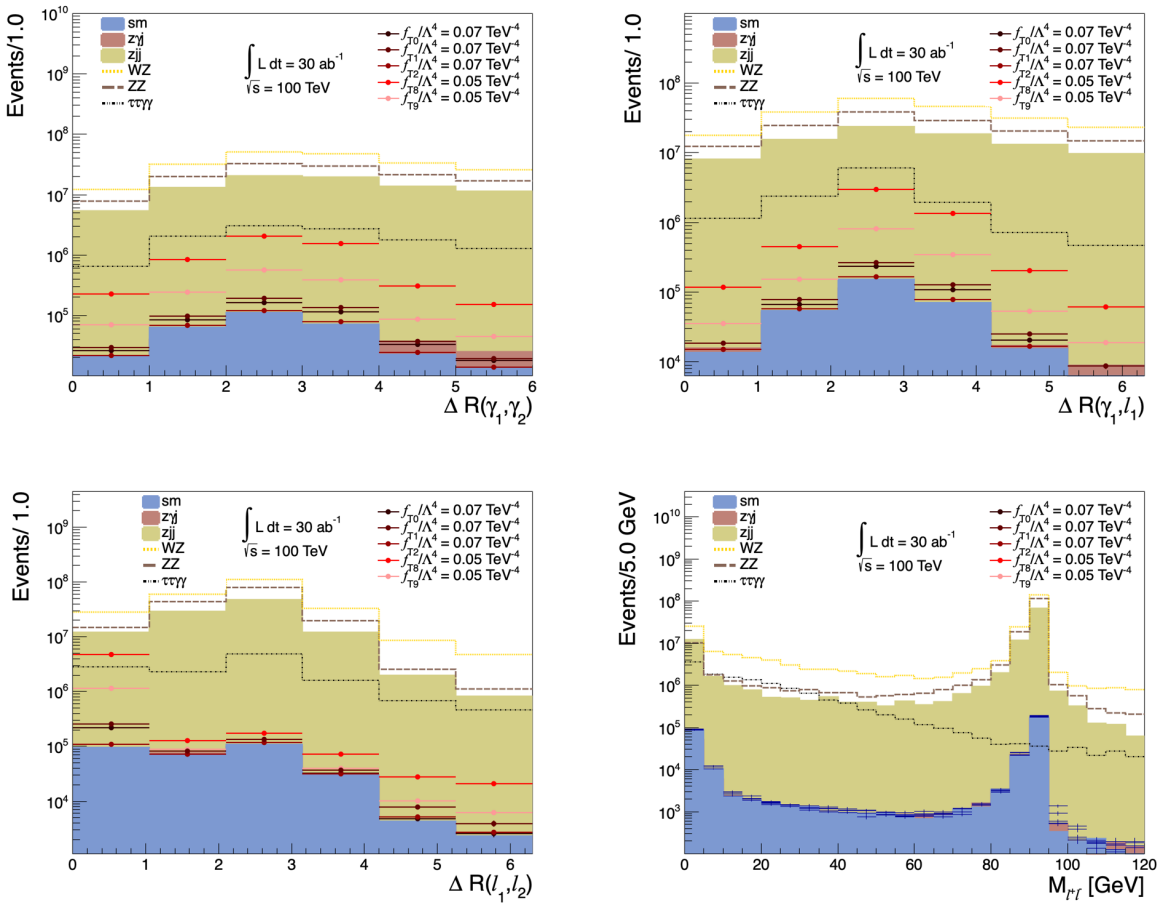


FIG. 10: Normalized $\Delta R(\gamma_1, \gamma_2)$, $\Delta R(\gamma_1, l_1)$, $\Delta R(l_1, l_2)$ and charged lepton pair invariant mass distribution after the event selection (Cut-0) for the signals and all relevant backgrounds processes at FCC-hh with L_{int} = 30 ab^{-1}.

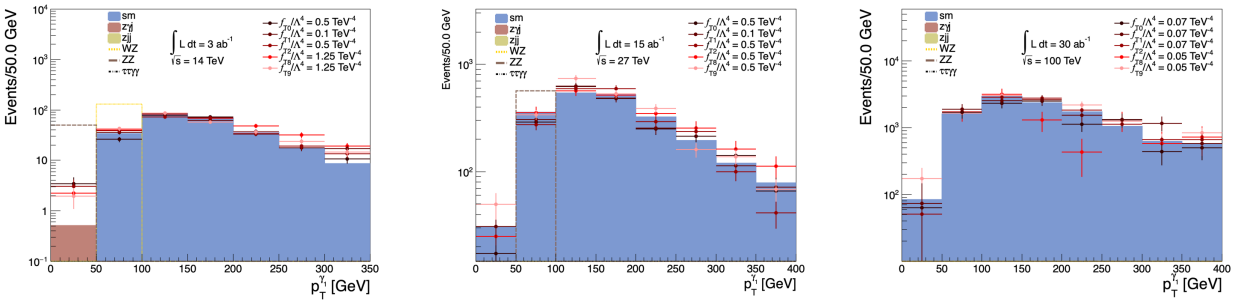


FIG. 11: Normalized distributions of transverse momentum of the leading photon (γ_1) after Cut-4 for the signals and all relevant backgrounds processes at HL-LHC, HE-LHC and FCC-hh with L_{int} = 3 ab^{-1}, 15 and 30 ab^{-1}, respectively

the coefficients of one nonzero operator at a time without UV bound are given in Table IV for HL-LHC, HE-LHC and FCC-hh collider options. This table also presents limits with δ_{sys}= 0, 3%, 5% and 10% systematic errors as well as the unitarity bounds defined as the scattering energy at which the aQGC coupling strength is set equal to the observed limit. Following the second way discussed above, we present obtained limits at 95% C.L. with UV bound applied on the invariant mass distribution of $l^+l^-\gamma\gamma$ system for HL-LHC, HE-LHC and FCC-hh collider options without systematic errors in Fig. 13 where the impact of the UV bound can be seen. The limits on the aQGCs with UV bounds get worsen as expected since the interference of the SM amplitude with the dimension-eight operators suppresses the square contribution of new physics amplitude.

We point out that our numerical results for the case f_{T8}/Λ^4 and f_{T9}/Λ^4 at HL-LHC agree with that of tri-boson production with an upgraded ATLAS detector at a HL-LHC with an integrated luminosity of 3000 fb^{-1} at a center-of-mass energy of 14 TeV [31]. In terms of comparing our results with existent ones, we obtain [-0.22;0.21] and [-0.45;0.41] TeV $^{-4}$ for f_{T8}/Λ^4 and f_{T9}/Λ^4 while the projection limits of ATLAS collaboration are twice as much as our HL-LHC limits. As shown in Table IV, our results on f_{T0}/Λ^4, f_{T1}/Λ^4 and f_{T2}/Λ^4 (f_{T8}/Λ^4 and f_{T9}/Λ^4) for FCC-hh without systematic errors are rather striking as compared to the best experimental results obtained by CMS with 13 TeV data via different production channel [23, 24, 28] by one (two) order of magnitude. In the case of HE-LHC, we obtained one order better limits on f_{T8}/Λ^4 and f_{T9}/Λ^4 couplings while similar sensitivities on f_{T0}/Λ^4, f_{T1}/Λ^4 and f_{T2}/Λ^4 couplings compared to the experimental limits obtained from CMS collaboration. Considering the results of the CMS and ATLAS collaboration via the same production channel used in our analysis [7, 9], our obtained limits for all aQGC are one to three order of magnitude better as can be seen from the comparison of Table I and Table IV for HL-LHC, HE-LHC and FCC-hh, respectively. The 95% C.L. limits on f_{T0}/Λ^4 (f_{T1}/Λ^4) couplings from W^+W^-jj analysis for HL-LHC, HE-LHC [83] and FCC-hh [84] are reported as [-0.6,0.6] ([-0.4,0.4]), [-0.027,0.027] ([-0.016,0.016]) TeV $^{-4}$ and [-0.01,0.01] TeV $^{-4}$, respectively. Comparing our expected limits for f_{T0}/Λ^4 and f_{T1}/Λ^4 couplings, we obtain limits at the same order for HL-LHC as well as FCC-hh, while one order weaker for HE-LHC. When presenting a realistic physics potential of future colliders for the process $pp \to Z\gamma\gamma$, one should consider the effect of systematic uncertainties on the limits. The source of systematic uncertainties are mainly based on the cross section measurements of $pp \to Z\gamma\gamma$ process with leading-order (LO) or next to leading order (NLO) predictions [85] and higher order EW corrections, the uncertainty in integrated luminosity as well as electrons and jets misidentified as photons. In our study, we focus on LO predictions but do not investigate the impact and validity of these higher-order corrections on the signal and SM background processes.

Since the main purpose of this study is not to discuss sources of the systematic uncertainty in detail but to investigate the overall effects of the systematic uncertainty on the limits values of aQGC, we consider three different scenarios of systematic uncertainty. The 95% C.L. limit values without systematic uncertainties and with three different scenarios of systematic uncertainties as δ_{sys}= 3%, 5% and 10% for three different collider options are quoted in Table 5. The limits on the aQGC considered in this study with systematic error are weaker slightly when realistic systematic error is considered, e.g., compared with a 10% systematic error and without systematic error, sensitivity of f_{T9}/Λ^4 gets worsen by about 1.2%, 1.7% and 1.5% for HL-LHC, HE-LHC and FCC-hh, respectively. We expect two (one) order of magnitude better limits on f_{T8}/Λ^4 and f_{T9}/Λ^4 (f_{T0}/Λ^4, f_{T1}/Λ^4 and f_{T2}/Λ^4) than the current experimental results even with δ_{sys}= 10% systematical uncertainty for FCC-hh whereas comparable limits for f_{T0}/Λ^4, f_{T1}/Λ^4 and f_{T2}/Λ^4 for HE-LHC.

V. SUMMARY AND CONCLUSIONS

Studying on trilinear and quartic vector boson coupling defined by the $SU(2)_L \times U(1)_Y$ gauge symmetry within the framework of the Standard Model (SM) may lead to an additional confirmation of the model as well as give clues to the existence of new physics at a higher energy scale parameterized with higher-order operators in an Effective Field Theory (EFT). In addition, the possibility of future hadron-hadron colliders with high energy, high luminosity and a high detection expectation access can open a wide window for new physics research for any possible signs of new physics at a higher scale parameterized with higher order operators. In light of these motivations, we focused on the sensitivity of anomalous quartic gauge couplings at HL-LHC, HE-LHC and FCC-hh collider options with corresponding integrated luminosities of L_{int} = 3 ab^{-1}, 15 ab^{-1}, 30 ab $^{-1}$ via phenomenological analysis of $pp \to Z\gamma\gamma$ production process considering charged lepton decay channel of Z boson. Taking into account the detector effects of these three collider options with the corresponding DELPHES card, the detailed analysis of two leptons and two photons final states as well as the relevant backgrounds is performed using cut-based techniques. In order to determine the region of the phase space that the signal dominates the relevant background, the transverse momentum, pseudo-rapidity, angular ΔR distributions of the leptons and photons in the final state, as well as the invariant distributions of two leptons with opposite charges and same flavors were investigated for optimum kinematic cuts. The distributions of the leading photon transverse momentum and $l^-l^+\gamma\gamma$ invariant mass system were found to be sensitive indicators of anomalous quartic gauge couplings. Sensitivity of anomalous quartic gauge couplings which one

can hope to achieve in future HL-LHC, HE-LHC and FCC-hh collider experiments occurring at $ZZ\gamma\gamma$ and $Z\gamma\gamma\gamma$ vertices for 95% C.L. has performed with three systematic uncertainty scenario δ_{sys}= 3%, 5% and 10% using the $l^+l^-\gamma\gamma$ invariant mass system distributions. Since $\mathcal{O}_{T8}$ and $\mathcal{O}_{T9}$ give rise to aQGC containing only the neutral electroweak gauge bosons among the anomalous quartic operators, we reach the remarkable sensitivity on especially f_{T8}/Λ^4 and f_{T9}/Λ^4 couplings for HE-LHC and FCC-hh options comparing with current experimental results as seen from Table IV. If we have compared the current experimental limits with the results determined from this work, sensitivity on the couplings f_{T8}/Λ^4 and f_{T9}/Λ^4 (f_{T0}/Λ^4, f_{T1}/Λ^4 and f_{T2}/Λ^4) for FCC-hh without systematic errors with L_{int} = 30 ab^{-1} are two (one) order better than the current experimental limits obtained from different vector boson scattering process by CMS collaboration [23, 24, 28], while the HE-LHC results are one order better limits on f_{T8}/Λ^4 and f_{T9}/Λ^4 couplings but similar sensitivities on f_{T0}/Λ^4, f_{T1}/Λ^4 and f_{T2}/Λ^4 couplings with L_{int} = 15 ab^{-1}. Using UV bound on the invariant mass distribution of $l^+l^-\gamma\gamma$ system for HL-LHC, HE-LHC and FCC-hh collider options without systematic errors, obtained limits on aQGCs are strongly affected compared to those without UV bound at 95% C.L. Further improvements on the limits of aQGCs f_{Tx} can be achieved from analysis of vector boson scattering process at high energy colliders as well as using multivariate techniques.

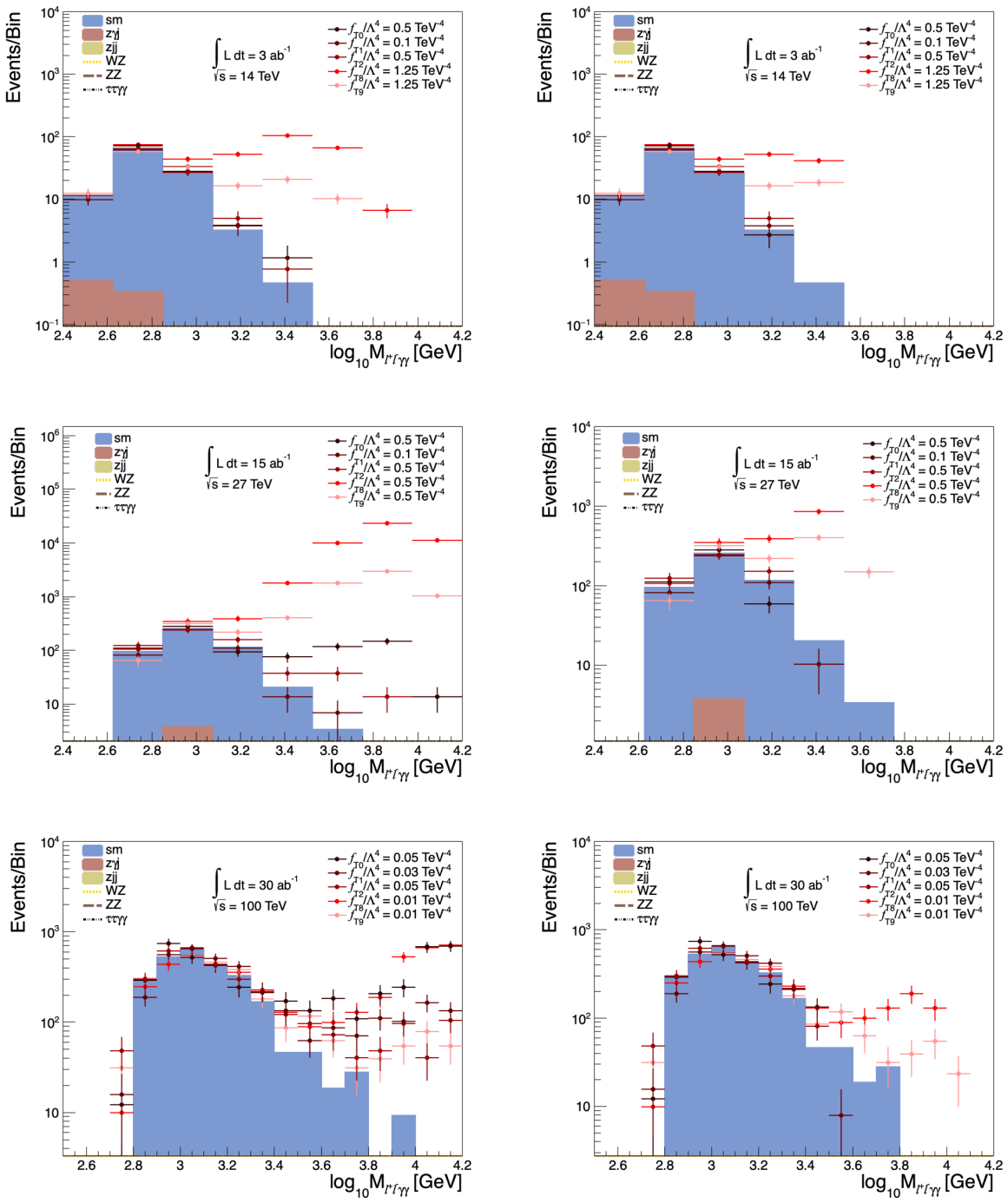


FIG. 12: Reconstructed mass of the leading and sub-leading charged leptons and photons after cut-5 without the UV bound (left panles) and with the UV bound (right panels) for the HL-LHC, HE-LHC and FCC-hh with an integrated luminosity of $L_{int} = 3$ ab^{-1}, 15 ab^{-1} and 30 ab^{-1}, respectively.

TABLE IV: 95% C.L. limits on anomalous quartic gauge couplings in units of TeV^{-4} and the unitarity bounds (Λ_{UV}) in units TeV considering δ_{sys}=0, 3%, 5% and 10% of systematic errors with an integrated luminosity of L_{int} = 3 ab^{-1}, 15 ab^{-1} and 30 ab^{-1} for the HL-LHC, HE-LHC and FCC-hh, respectively.

		HL-LHC		HE-LHC		FCC-hh	
	δ_{sys}	Limits [TeV^{-4}]	Λ_{UV}[TeV]	Limits [TeV^{-4}]	Λ_{UV}[TeV]	Limits [TeV^{-4}]	Λ_{UV}[TeV]
	0%	[-1.07;0.76]		[-1.89;1.29]$\times10^{-1}$		[-1.29;1.05]$\times10^{-2}$	
f_{T0}/Λ^4	3%	[-1.10;0.78]	1.4	[-2.04;1.44]$\times10^{-1}$	2.0	[-1.73;1.50]$\times10^{-2}$	3.6
	5%	[-1.14;0.82]		[-2.23;1.64]$\times10^{-1}$		[-2.11;1.87]$\times10^{-2}$	
	10%	[-1.28;0.96]		[-2.75;2.16]$\times10^{-1}$		[-2.86;2.63]$\times10^{-2}$	
	0%	[-0.92;0.72]		[-1.76;1.40]$\times10^{-1}$		[-1.34;0.83]$\times10^{-2}$	
f_{T1}/Λ^4	3%	[-0.94;0.74]	1.6	[-1.91;1.56]$\times10^{-1}$	2.3	[-1.75;1.23]$\times10^{-2}$	4.5
	5%	[-0.97;0.78]		[-2.11;1.76]$\times10^{-1}$		[-2.08;1.56]$\times10^{-2}$	
	10%	[-1.10;0.91]		[-2.64;2.29]$\times10^{-1}$		[-2.76;2.24]$\times10^{-2}$	
	0%	[-0.97;0.94]		[-4.99;2.75]$\times10^{-1}$		[-2.15;1.52]$\times10^{-2}$	
f_{T2}/Λ^4	3%	[-0.99;0.97]	1.6	[-5.35;3.11]$\times10^{-1}$	2.2	[-2.83;2.20]$\times10^{-2}$	4.3
	5%	[-1.04;1.01]		[-5.81;3.57]$\times10^{-1}$		[-3.40;2.78]$\times10^{-2}$	
	10%	[-1.19;1.15]		[-7.07;4.82]$\times10^{-1}$		[-4.57;3.94]$\times10^{-2}$	
	0%	[-2.19;2.11]$\times10^{-1}$		[-3.74;2.77]$\times10^{-2}$		[-1.16;0.54]$\times10^{-3}$	
f_{T8}/Λ^4	3%	[-2.25;2.17]$\times10^{-1}$	3.9	[-4.04;3.07]$\times10^{-2}$	6.5	[-1.33;0.71]$\times10^{-3}$	17.2
	5%	[-2.35;2.26]$\times10^{-1}$		[-4.44;3.47]$\times10^{-2}$		[-1.50;0.89]$\times10^{-3}$	
	10%	[-2.68;2.60]$\times10^{-1}$		[-5.51;4.54]$\times10^{-2}$		[-1.90;0.13]$\times10^{-3}$	
	0%	[-4.46;4.10]$\times10^{-1}$		[-6.83;4.83]$\times10^{-2}$		[-1.26;1.09]$\times10^{-3}$	
f_{T9}/Λ^4	3%	[-4.58;4.22]$\times10^{-1}$	4.1	[-7.39;5.39]$\times10^{-2}$	6.9	[-1.35;1.18]$\times10^{-3}$	17.7
	5%	[-4.76;4.40]$\times10^{-1}$		[-8.11;6.11]$\times10^{-2}$		[-1.48;1.31]$\times10^{-3}$	
	10%	[-5.41;5.05]$\times10^{-1}$		[-10.05;8.06]$\times10^{-2}$		[-1.84;1.66]$\times10^{-3}$	

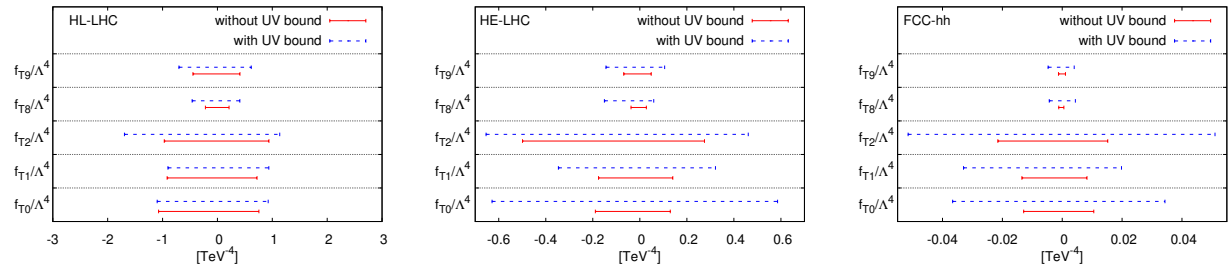


FIG. 13: 95% C.L. limits on anomalous quartic gauge couplings with and without the unitarity bounds (Λ_{UV}) considering δ_{sys}=0 of systematic errors with an integrated luminosity of L_{int} = 3 ab^{-1}, 15 ab^{-1} and 30 ab^{-1} for the HL-LHC, HE-LHC and FCC-hh, respectively.

Acknowledgments

This work was supported by the Scientific and Technological Research Council of Turkey (TUBITAK), Grand No: 120F055.

Appendix A: Dimension-eight operators for Anomalous Quartic Gauge Couplings

The anomalous quartic gauge couplings come out from dimension-8 operators [70–72]. There are three classes of operators containing either covariant derivatives of Higgs doublet ($D_\mu\Phi$) only, or two field strength tensors and two $D_\mu\Phi$, or field strength tensors only;

i) Two independent operators containing either covariant derivatives of Higgs doublet ($D_\mu\Phi$) only:

$$\mathcal{O}_{S0} = [(D_\mu\Phi)^\dagger D_\nu\Phi] \times [(D^\mu\Phi)^\dagger D^\nu\Phi], \tag{A1}$$

$$\mathcal{O}_{S1} = [(D_\mu\Phi)^\dagger D_\mu\Phi] \times [(D^\nu\Phi)^\dagger D^\nu\Phi], \tag{A2}$$

ii) Seven operators are related to $D_\mu\Phi$ and the field strength are given by

$$\mathcal{O}_{M0} = Tr[W_{\mu\nu}W^{\mu\nu}] \times [(D_\beta\Phi)^\dagger D^\beta\Phi], \tag{A3}$$

$$\mathcal{O}_{M1} = Tr[W_{\mu\nu}W^{\nu\beta}] \times [(D_\beta\Phi)^\dagger D^\mu\Phi], \tag{A4}$$

$$\mathcal{O}_{M2} = [B_{\mu\nu}B^{\mu\nu}] \times [(D_\beta\Phi)^\dagger D^\beta\Phi], \tag{A5}$$

$$\mathcal{O}_{M3} = [B_{\mu\nu}B^{\nu\beta}] \times [(D_\beta\Phi)^\dagger D^\mu\Phi], \tag{A6}$$

$$\mathcal{O}_{M4} = [(D_\mu\Phi)^\dagger W_{\beta\nu}D^\mu\Phi] \times B^{\beta\nu}, \tag{A7}$$

$$\mathcal{O}_{M5} = [(D_\mu\Phi)^\dagger W_{\beta\nu}D^\nu\Phi] \times B^{\beta\mu}, \tag{A8}$$

$$\mathcal{O}_{M6} = [(D_\mu\Phi)^\dagger W_{\beta\nu}W^{\beta\nu}D^\mu\Phi], \tag{A9}$$

$$\mathcal{O}_{M7} = [(D_\mu\Phi)^\dagger W_{\beta\nu}W^{\beta\mu}D^\nu\Phi]. \tag{A10}$$

where the field strength tensor of the $SU(2)$ ($W_{\mu\nu}$) and $U(1)$ ($B_{\mu\nu}$) are given by

$$\begin{aligned} W_{\mu\nu} &= \frac{i}{2}g\tau^i(\partial_\mu W^i_\nu - \partial_\nu W^i_\mu + g\epsilon_{ijk}W^j_\mu W^k_\nu) \\ B_{\mu\nu} &= \frac{i}{2}g'(\partial_\mu B_\nu - \partial_\nu B_\mu). \end{aligned} \tag{A11}$$

Here, $\tau^i (i = 1, 2, 3)$ are the $SU(2)$ generators, $g = e/sin\theta_W$, $g' = g/cos\theta_W$, e is the unit of electric charge and θ_W is the Weinberg angle.

TABLE V: Quartic gauge boson vertices modified by the related dimension-8 operator are marked with ✓ [72].

	$WWWW$	$WWZZ$	$ZZZZ$	$WW\gamma Z$	$WW\gamma\gamma$	$ZZZ\gamma$	$ZZ\gamma\gamma$	$Z\gamma\gamma\gamma$	$\gamma\gamma\gamma\gamma$
$\mathcal{O}_{S0}, \mathcal{O}_{S1}$	✓	✓	✓						
$\mathcal{O}_{M0}, \mathcal{O}_{M1}, \mathcal{O}_{M6}\mathcal{O}_{M7}$	✓	✓	✓	✓	✓	✓	✓		
$\mathcal{O}_{M2}, \mathcal{O}_{M3}, \mathcal{O}_{M4}, \mathcal{O}_{M5}$		✓	✓	✓	✓	✓	✓		
$\mathcal{O}_{T0}, \mathcal{O}_{T1}, \mathcal{O}_{T2}$	✓	✓	✓	✓	✓	✓	✓	✓	✓
$\mathcal{O}_{T5}, \mathcal{O}_{T6}, \mathcal{O}_{T7}$		✓	✓	✓	✓	✓	✓	✓	✓
$\mathcal{O}_{T8}, \mathcal{O}_{T9}$			✓			✓	✓	✓	✓

iii) Eight operators containing field strength tensors only are as follows

$$\mathcal{O}_{T0} = \mathrm{Tr}[W_{\mu\nu}W^{\mu\nu}] \times \mathrm{Tr}[W_{\alpha\beta}W^{\alpha\beta}] \tag{A12}$$

$$\mathcal{O}_{T1} = \mathrm{Tr}[W_{\alpha\nu}W^{\mu\beta}] \times \mathrm{Tr}[W_{\mu\beta}W^{\alpha\nu}] \tag{A13}$$

$$\mathcal{O}_{T2} = \mathrm{Tr}[W_{\alpha\mu}W^{\mu\beta}] \times \mathrm{Tr}[W_{\beta\nu}W^{\nu\alpha}] \tag{A14}$$

$$\mathcal{O}_{T5} = \mathrm{Tr}[W_{\mu\nu}W^{\mu\nu}] \times B_{\alpha\beta}B^{\alpha\beta} \tag{A15}$$

$$\mathcal{O}_{T6} = \mathrm{Tr}[W_{\alpha\nu}W^{\mu\beta}] \times B_{\mu\beta}B^{\alpha\nu} \tag{A16}$$

$$\mathcal{O}_{T7} = \mathrm{Tr}[W_{\alpha\mu}W^{\mu\beta}] \times B_{\beta\nu}B^{\nu\alpha} \tag{A17}$$

$$\mathcal{O}_{T8} = [B_{\mu\nu}B^{\mu\nu}B_{\alpha\beta}B^{\alpha\beta}] \tag{A18}$$

$$\mathcal{O}_{T9} = [B_{\alpha\mu}B^{\mu\beta}B_{\beta\nu}B^{\nu\alpha}] \tag{A19}$$

A complete list of corresponding quartic gauge boson vertices modified by dimension-8 operators is given in Table V.

[1] G. Aad *et al.* [ATLAS Collaboration], Phys. Lett. B **716**, 1 (2012) [arXiv:1207.7214 [hep-ex]].

[2] S. Chatrchyan *et al.* [CMS Collaboration], Phys. Lett. B **716**, 30 (2012) [arXiv:1207.7235 [hep-ex]].

[3] G. Belanger and F. Boudjema, Phys. Lett. B **288**, 201-209 (1992)

[4] O. J. P. Eboli, M. C. Gonzalez-Garcia and S. M. Lietti, Phys. Rev. D **69**, 095005 (2004) [arXiv:hep-ph/0310141 [hep-ph]].

[5] P. Achard *et al.* [L3], Phys. Lett. B **540**, 43-51 (2002) [arXiv:hep-ex/0206050 [hep-ex]].

[6] G. Abbiendi *et al.* [OPAL], Phys. Rev. D **70**, 032005 (2004) [arXiv:hep-ex/0402021 [hep-ex]].

[7] G. Aad *et al.* [ATLAS], Phys. Rev. D **93**, no.11, 112002 (2016) [arXiv:1604.05232 [hep-ex]].

[8] A. M. Sirunyan *et al.* [CMS], JHEP **10**, 072 (2017) [arXiv:1704.00366 [hep-ex]].

[9] A. Tumasyan *et al.* [CMS], [arXiv:2105.12780 [hep-ex]].

[10] B. Abbott *et al.* [D0], Phys. Rev. D **62**, 052005 (2000) [arXiv:hep-ex/9912033 [hep-ex]].

[11] V. M. Abazov *et al.* [D0], Phys. Rev. D **88**, 012005 (2013) [arXiv:1305.1258 [hep-ex]].

[12] G. Aad *et al.* [ATLAS], Phys. Rev. Lett. **113**, no.14, 141803 (2014) [arXiv:1405.6241 [hep-ex]].

[13] G. Aad *et al.* [ATLAS], Phys. Rev. Lett. **115**, no.3, 031802 (2015) [arXiv:1503.03243 [hep-ex]].

[14] M. Aaboud *et al.* [ATLAS], Phys. Rev. D **96**, no.1, 012007 (2017) [arXiv:1611.02428 [hep-ex]].

[15] M. Aaboud *et al.* [ATLAS], Eur. Phys. J. C **77**, no.9, 646 (2017) [arXiv:1707.05597 [hep-ex]].

[16] M. Aaboud *et al.* [ATLAS], Phys. Rev. D **95**, no.3, 032001 (2017) [arXiv:1609.05122 [hep-ex]].

[17] S. Chatrchyan *et al.* [CMS], Phys. Rev. D **90**, no.3, 032008 (2014) [arXiv:1404.4619 [hep-ex]].

[18] A. M. Sirunyan *et al.* [CMS], Phys. Lett. B **774**, 682-705 (2017) [arXiv:1708.02812 [hep-ex]].

[19] V. Khachatryan *et al.* [CMS], Phys. Lett. B **770**, 380-402 (2017) [arXiv:1702.03025 [hep-ex]].

[20] V. Khachatryan *et al.* [CMS], JHEP **06**, 106 (2017) [arXiv:1612.09256 [hep-ex]].

[21] A. M. Sirunyan *et al.* [CMS], Phys. Rev. Lett. **120**, no.8, 081801 (2018) [arXiv:1709.05822 [hep-ex]].

[22] A. M. Sirunyan *et al.* [CMS], Phys. Lett. B **795**, 281-307 (2019) [arXiv:1901.04060 [hep-ex]].

[23] A. M. Sirunyan *et al.* [CMS], Phys. Lett. B **798**, 134985 (2019) [arXiv:1905.07445 [hep-ex]].

[24] A. M. Sirunyan *et al.* [CMS], Phys. Lett. B **812**, 135992 (2021) [arXiv:2008.07013 [hep-ex]].

[25] A. M. Sirunyan *et al.* [CMS], JHEP **06**, 076 (2020) [arXiv:2002.09902 [hep-ex]].

[26] A. M. Sirunyan *et al.* [CMS], Phys. Lett. B **809**, 135710 (2020) [arXiv:2005.01173 [hep-ex]].

[27] A. M. Sirunyan *et al.* [CMS], Phys. Lett. B **811**, 135988 (2020) [arXiv:2008.10521 [hep-ex]].

[28] A. Tumasyan *et al.* [CMS], [arXiv:2106.11082 [hep-ex]].

[29] C. Degrande, J. L. Holzbauer, S. C. Hsu, A. V. Kotwal, S. Li, M. Marx, O. Mattelaer, J. Metcalfe, M. A. Pleier and C. Pollard, *et al.* [arXiv:1309.7452 [physics.comp-ph]].

[30] A. Gutierrez-Rodriguez, C. G. Honorato, J. Montano and M. A. Pérez, Phys. Rev. D **89**, no.3, 034003 (2014) [arXiv:1304.7410 [hep-ph]].

[31] [ATLAS], ATL-PHYS-PUB-2013-006.

[32] A. S. Kurova and E. Y. Soldatov, Phys. Atom. Nucl. **80**, no.4, 725-729 (2017)

[33] A. S. Kurova and E. Y. Soldatov, J. Phys. Conf. Ser. **798**, no.1, 012097 (2017)

[34] A. S. Belyaev, O. J. P. Eboli, M. C. Gonzalez-Garcia, J. K. Mizukoshi, S. F. Novaes and I. Zacharov, Phys. Rev. D **59**, 015022 (1999) [arXiv:hep-ph/9805229 [hep-ph]].

[35] O. J. P. Eboli, M. C. Gonzalez-Garcia, S. M. Lietti and S. F. Novaes, Phys. Rev. D **63**, 075008 (2001) [arXiv:hep-ph/0009262 [hep-ph]].

[36] G. Perez, M. Sekulla and D. Zeppenfeld, Eur. Phys. J. C **78**, no.9, 759 (2018) [arXiv:1807.02707 [hep-ph]].

[37] Y. C. Guo, Y. Y. Wang and J. C. Yang, Nucl. Phys. B **961**, 115222 (2020) [arXiv:1912.10686 [hep-ph]].

[38] Y. C. Guo, Y. Y. Wang, J. C. Yang and C. X. Yue, Chin. Phys. C **44**, no.12, 123105 (2020) [arXiv:2002.03326 [hep-ph]].

[39] D. Yang, Y. Mao, Q. Li, S. Liu, Z. Xu and K. Ye, JHEP **04**, 108 (2013) [arXiv:1211.1641 [hep-ph]].

[40] K. Ye, D. Yang and Q. Li, Phys. Rev. D **88**, 015023 (2013) [arXiv:1305.5979 [hep-ph]].

[41] Y. Wen, H. Qu, D. Yang, Q. s. Yan, Q. Li and Y. Mao, JHEP **03**, 025 (2015) [arXiv:1407.4922 [hep-ph]].

[42] J. W. Zhu, R. Y. Zhang, W. G. Ma, Q. Yang and Y. Jiang, J. Phys. G **47**, no.5, 055006 (2020) [arXiv:2005.10707 [hep-ph]].

[43] V. Ari, E. Gurkanli, M. Köksal, A. Gutiérrez-Rodríguez and M. A. Hernández-Ruíz, [arXiv:2104.00474 [hep-ph]].

[44] O. Kepka and C. Royon, Phys. Rev. D **78**, 073005 (2008) [arXiv:0808.0322 [hep-ph]].

[45] E. Chapon, C. Royon and O. Kepka, [arXiv:0908.1061 [hep-ph]].

[46] E. Chapon, C. Royon and O. Kepka, Phys. Rev. D **81**, 074003 (2010) [arXiv:0912.5161 [hep-ph]].

[47] R. S. Gupta, Phys. Rev. D **85**, 014006 (2012) [arXiv:1111.3354 [hep-ph]].

[48] S. Fichet, G. von Gersdorff, B. Lenzi, C. Royon and M. Saimpert, JHEP **02**, 165 (2015) [arXiv:1411.6629 [hep-ph]].

[49] C. Baldenegro, S. Fichet, G. von Gersdorff and C. Royon, JHEP **06**, 142 (2017) [arXiv:1703.10600 [hep-ph]].

[50] S. Tizchang and S. M. Etesami, JHEP **07**, 191 (2020) [arXiv:2004.12203 [hep-ph]].

[51] O. J. P. Eboli, M. C. Gonzalez-Garcia and S. F. Novaes, Nucl. Phys. B **411**, 381-396 (1994) [arXiv:hep-ph/9306306 [hep-ph]].

[52] O. J. P. Eboli, M. B. Magro, P. G. Mercadante and S. F. Novaes, Phys. Rev. D **52**, 15-21 (1995) [arXiv:hep-ph/9503432 [hep-ph]].

[53] J. L. Hewett and F. J. Petriello, Phys. Rev. D **64**, 095017 (2001) [arXiv:hep-ph/0105106 [hep-ph]].

[54] O. J. P. Eboli and J. K. Mizukoshi, Phys. Rev. D **64**, 075011 (2001) [arXiv:hep-ph/0105238 [hep-ph]].

[55] A. Senol and M. Köksal, Phys. Lett. B **742**, 143-148 (2015) [arXiv:1410.3648 [hep-ph]].

[56] V. D. Barger, T. Han and R. J. N. Phillips, Phys. Rev. D **39**, 146 (1989)

[57] A. Brunstein, O. J. P. Eboli and M. C. Gonzalez-Garcia, Phys. Lett. B **375**, 233-239 (1996) [arXiv:hep-ph/9602264 [hep-ph]].

[58] T. Han, H. J. He and C. P. Yuan, Phys. Lett. B **422**, 294-304 (1998) [arXiv:hep-ph/9711429 [hep-ph]].

[59] O. J. P. Eboli, M. C. Gonzalez-Garcia and J. K. Mizukoshi, Phys. Rev. D **58**, 034008 (1998) [arXiv:hep-ph/9711499 [hep-ph]].

[60] W. J. Stirling and A. Werthenbach, Eur. Phys. J. C **14**, 103-110 (2000) [arXiv:hep-ph/9903315 [hep-ph]].

[61] W. J. Stirling and A. Werthenbach, Phys. Lett. B **466**, 369-374 (1999) [arXiv:hep-ph/9907235 [hep-ph]].

[62] G. Belanger, F. Boudjema, Y. Kurihara, D. Perret-Gallix and A. Semenov, Eur. Phys. J. C **13**, 283-293 (2000) [arXiv:hep-ph/9908254 [hep-ph]].

[63] F. Gangemi, [arXiv:hep-ph/0002142 [hep-ph]].

[64] A. Denner, S. Dittmaier, M. Roth and D. Wackeroth, Eur. Phys. J. C **20**, 201-215 (2001) [arXiv:hep-ph/0104057 [hep-ph]].

[65] G. Montagna, M. Moretti, O. Nicrosini, M. Osmo and F. Piccinini, Phys. Lett. B **515**, 197-205 (2001)

[arXiv:hep-ph/0105120 [hep-ph]].

[66] M. Köksal, Mod. Phys. Lett. A **29**, no.34, 1450184 (2014) [arXiv:1402.3112 [hep-ph]].

[67] I. Zurbano Fernandez, M. Zobov, A. Zlobin, F. Zimmermann, M. Zerlauth, C. Zanoni, C. Zannini, O. Zagorodnova, I. Zacharov and M. Yu, *et al.* "High-Luminosity Large Hadron Collider (HL-LHC): Technical design report," doi:10.23731/CYRM-2020-0010

[68] A. Abada *et al.* [FCC], Eur. Phys. J. ST **228**, no.5, 1109-1382 (2019)

[69] A. Abada *et al.* [FCC], Eur. Phys. J. ST **228**, no.4, 755-1107 (2019)

[70] O. J. P. Eboli, M. C. Gonzalez-Garcia and J. K. Mizukoshi, Phys. Rev. D **74**, 073005 (2006) [arXiv:hep-ph/0606118 [hep-ph]].

[71] C. Degrande, O. Eboli, B. Feigl, B. Jäger, W. Kilian, O. Mattelaer, M. Rauch, J. Reuter, M. Sekulla and D. Wackeroth, [arXiv:1309.7890 [hep-ph]].

[72] M. Baak, A. Blondel, A. Bodek, R. Caputo, T. Corbett, C. Degrande, O. Eboli, J. Erler, B. Feigl and A. Freitas, *et al.* [arXiv:1310.6708 [hep-ph]].

[73] K. Arnold, M. Bahr, G. Bozzi, F. Campanario, C. Englert, T. Figy, N. Greiner, C. Hackstein, V. Hankele and B. Jager, *et al.* Comput. Phys. Commun. **180**, 1661-1670 (2009) [arXiv:0811.4559 [hep-ph]].

[74] J. Alwall, R. Frederix, S. Frixione, V. Hirschi, F. Maltoni, O. Mattelaer, H. S. Shao, T. Stelzer, P. Torrielli and M. Zaro, JHEP **07** (2014), 079 [arXiv:1405.0301 [hep-ph]].

[75] A. Alloul, N. D. Christensen, C. Degrande, C. Duhr and B. Fuks, Comput. Phys. Commun. **185** (2014), 2250-2300 [arXiv:1310.1921 [hep-ph]].

[76] C. Degrande, C. Duhr, B. Fuks, D. Grellscheid, O. Mattelaer and T. Reiter, Comput. Phys. Commun. **183** (2012), 1201-1214 [arXiv:1108.2040 [hep-ph]].

[77] T. Sjöstrand, S. Ask, J. R. Christiansen, R. Corke, N. Desai, P. Ilten, S. Mrenna, S. Prestel, C. O. Rasmussen and P. Z. Skands, Comput. Phys. Commun. **191** (2015), 159-177 [arXiv:1410.3012 [hep-ph]].

[78] J. de Favereau *et al.* [DELPHES 3], JHEP **02** (2014), 057 [arXiv:1307.6346 [hep-ex]].

[79] M. Cacciari, G. P. Salam and G. Soyez, Eur. Phys. J. C **72**, 1896 (2012)[arXiv:1111.6097 [hep-ph]].

[80] M. Cacciari, G. P. Salam and G. Soyez, JHEP **0804**, 063 (2008) [arXiv:0802.1189 [hep-ph]].

[81] ATLAS collaboration, Tech. Rep. ATL-PHYS-PUB-2016-026.

[82] M. L. Mangano, G. Ortona and M. Selvaggi, Eur. Phys. J. C **80**, no.11, 1030 (2020) [arXiv:2004.03505 [hep-ph]].

[83] P. Azzi, S. Farry, P. Nason, A. Tricoli, D. Zeppenfeld, R. Abdul Khalek, J. Alimena, N. Andari, L. Aperio Bella and A. J. Armbruster, *et al.* CERN Yellow Rep. Monogr. **7**, 1-220 (2019) arXiv:1902.04070 [hep-ph]].

[84] B. Jager, L. Salfelder, M. Worek and D. Zeppenfeld, Phys. Rev. D **96**, no.7, 073008 (2017) [arXiv:1704.04911 [hep-ph]].

[85] G. Bozzi, F. Campanario, M. Rauch and D. Zeppenfeld, Phys. Rev. D **84**, 074028 (2011) [arXiv:1107.3149 [hep-ph]].